Nonradiative Energy Transfer through Distributed Bands in Piezochemically-synthesized Cesium and Formamidinium Lead Halide Perovskites

Sankaramangalam Balachandran Bhagyalakshmi, Sushant Ghimire,* Kiyonari Takahashi, Ken-ichi Yuyama, Yuta Takano, Takayoshi Nakamura and Vasudevanpillai Biju*

Research Institute for Electronic Science and Graduate School of Environmental Science, Hokkaido University N20, W10, Sapporo, Hokkaido 001-0020, JAPAN

*Address correspondence to: ghimiresushant@eis.hokudai.ac.jp, biju@es.hokudai.ac.jp

Abstract: Repeated absorption of emitted photons, also called photon recycling, in large crystals and thick films of perovskites leads to delayed photoluminescence (PL) and decrease of PL intensity. The role of distinct bandgaps, which act as donors and acceptors of energy, and nonradiative energy transfer on such delayed, low intensity emission is yet to be rationalized. Here we report delayed emission by nonradiative energy transfer across a distribution of energy states in close-packed crystallites of cesium lead bromide ($CsPbBr_3$), formamidinium lead bromide ($FAPbBr_3$), or the mixed halide [$FAPb(BrI)_3$] perovskite synthesized in the form of thick pellets by the piezochemical method. The PL lifetime of the bromide-rich domain in the mixed halide pellet is considerably decreased when compared with a pure $FAPbBr_3$ pellet. Here the domains with higher bromide composition act as the energy donor, whereas the iodide-rich domains are the acceptors. Time-resolved PL measurements of $CsPbBr_3$, $FAPbBr_3$, and the mixed halide $FAPb(BrI)_3$ perovskite pellets help us to clarify the role of nonradiative energy transfer on photon recycling.

Keywords: perovskite, piezochemistry, energy transfer, photoluminescence, photon recycling

Rapid advancement in the electrooptical and photovoltaic technologies transpires with the development of lead halide perovskites, which is owing to their excellent optical and charge

carrier properties. These perovskites form active parts of solar cells, [1a,b] LEDs, [1c,d] lasers, [1e,f] and optical detectors.[1g,h] In particular, the low exciton binding energy and long-range diffusion of photogenerated charge carriers make them promising for heterojunction solar cells.[2] Recently, photon recycling in perovskites is proposed to have a positive impact to solar cells.[3a,b] This recycling phenomenon occurs in the bulk films and large crystals of perovskites, which is the result of repeated absorption and emission of photons.[3c,d,e,f] Thus, the effective PL lifetime increases in such samples. For example, Motti *et al.* detected an increase in PL lifetime from 4 ns to 1 μs or longer in a quasi-two-dimensional (2D)/3D lead iodide perovskite film,[3f] which is due to the reabsorption of photons emitted from the higher bandgap quasi-2D layer by the lower bandgap 3D layer.

Apart from the multiple radiative absorption-emission events in photon recycling, the distribution of energy states or bandgaps should facilitate nonradiative energy transfer. Energy cascading is known for compositionally homogenous perovskite aggregates and films, which takes place across different crystallites with closely-spaced energy states.[3f,4] In samples with varied perovskite compositions, energy transfer takes place from the larger bandgap (donor) to the smaller bandgap (acceptor) parts, which is assigned to Förster resonance energy transfer (FRET).[5] Nonetheless, the relations of nonradiative energy transfer in pure and mixed halide perovskites to delayed emission remain poorly understood. Although we recently detected nonradiative energy transfer from bromide to iodide perovskites,[6] the energy transfer through

a distribution of closely-spaced energy states in close-packed pure halide perovskite is intriguing. In this work, we find delayed emission by photon recycling through nonradiative energy transfer across continuous donor-acceptor states, which is by preparing pure $CsPbBr_3$ or $FAPbBr_3$, or mixed halide $FAPb(BrI)_3$ perovskite samples. These samples are prepared by the piezochemical method by applying the pressure to the respective precursor solid solutions, providing submicron-to-micron size crystallites closely packed. The samples are characterized by X-ray diffraction (XRD), diffused reflectance, and PL measurements. We confirm the distribution of bandgaps in close-packed pure halide perovskites by the measurement of PL maxima of isolated crystallites. Distinct PL maxima ranging from ca 530 nm to ca 560 nm are detected for different crystallites collected from a $FAPbBr_3$ pellet. The mixed halide $FAPb(BrI)_3$ perovskite with distinct bromide- (donor) and iodide-(acceptor) regions help us to assign the delayed emission by photon recycling to nonradiative energy transfer.

The role of mechanical force in synthesizing perovskites is well known.[7] Combined with this fact and the abundance of silicate perovskites in the mantle of Earth,[8] we utilized pressure as the reaction force in the preparation and close-packing of $CsPbBr_3$ and $FAPbBr_3$ perovskites. A scheme of synthesis of these samples is shown in Figure 1. Details of synthesis and characterization of $CsPbBr_3$, $FAPbBr_3$ and $FAPb(BrI)_3$ are provided in the Experimental Section. We characterized these perovskite samples by X-ray diffraction (XRD) studies and by comparing the XRD patterns in the literature. Figure 2a (iv) and (v) are the XRD patterns of

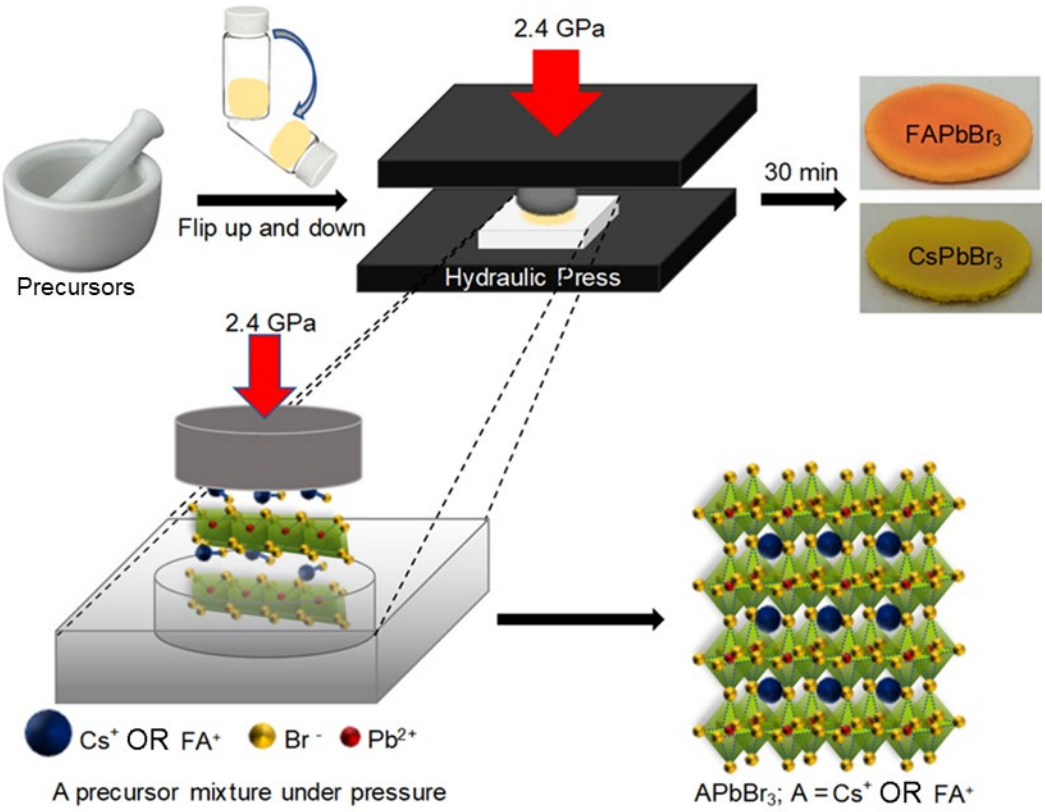

Figure 1. A scheme of synthesis and close-packing of $CsPbBr_3$ or $FAPbBr_3$ perovskite samples.

$CsPbBr_3$ and $FAPbBr_3$ perovskites, respectively. The diffraction peaks of $CsPbBr_3$ are assigned to the cubic *Pm3m* crystal phase, according to the literature[4c] and the standard ICSD card no #29073. Here, the peaks at 15.05°, 21.48°, 30.63°, 33.96°, 37.92°, 44.10° and 48.55° are in agreement with the (100), (110), (200), (210), (211), (220) and (310) crystal planes, respectively. Similarly, $FAPbBr_3$ sample is in the cubic phase with the diffraction peaks at 14.80°, 21.60°, 30.50°, 33.84°, 37.92°, 40.89° and 44.22°, which correspond to the (100), (110), (200), (210), (211), (220) and (300) crystal planes, respectively.[9] Small amounts of unreacted precursors, which show characteristic XRD peaks, are also present. As the

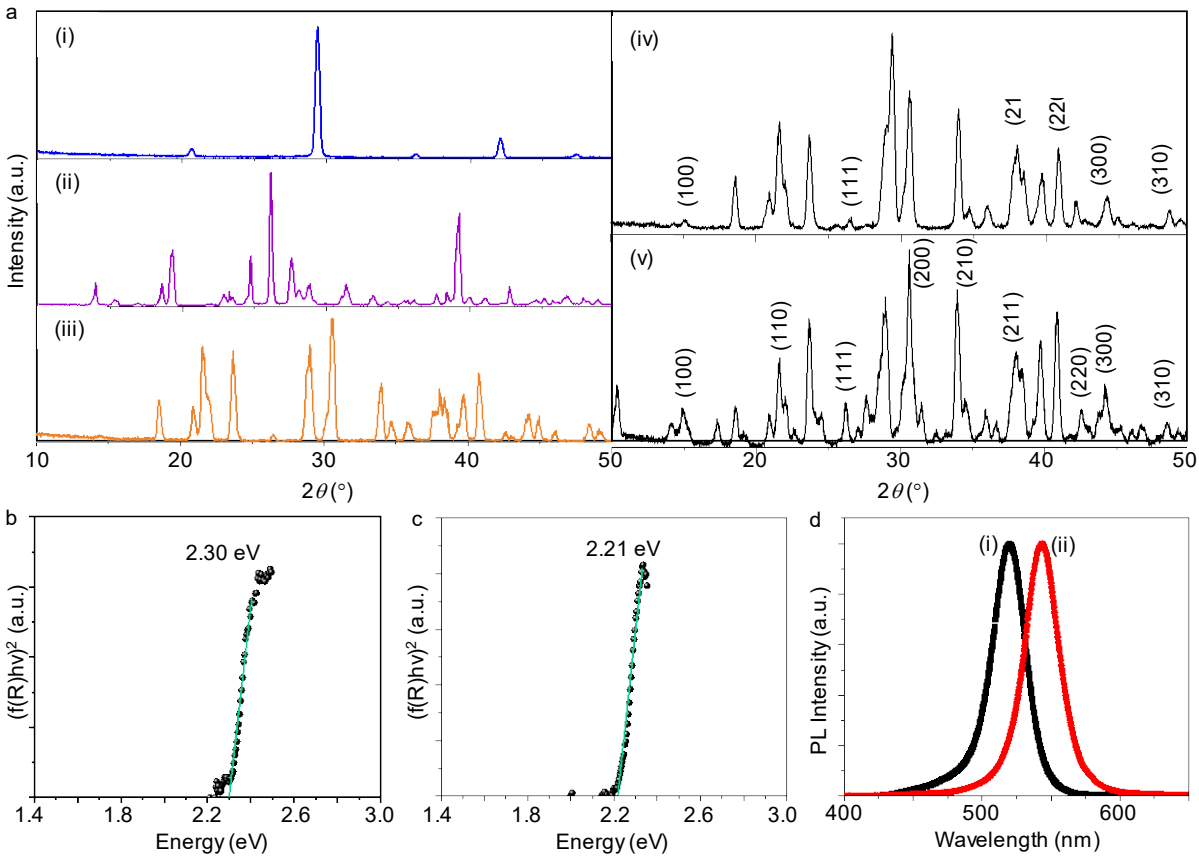

Figure 2. **The structural and optical characteristics of perovskite pellets.** (a) Powder XRD patterns of (i-iii) perovskite precursors [(i) CsBr, (ii) FABr, (iii) $PbBr_2$], and (iv,v) perovskite pellets [(iv) $CsPbBr_3$ and (v) $FAPbBr_3$]. (b,c) Tauc plots of (b) $CsPbBr_3$ and (c) $FAPbBr_3$ perovskite pellets. (d) PL spectra of isolated crystallites of (i) $CsPbBr_3$ and (ii) $FAPbBr_3$ perovskites.

references, the XRD patterns of precursors are shown in Figure 2a (i to iii). The diffraction peaks at 29.27°and 42.00° match with CsBr, those at 29.02°, 30.50°, 33.84°, 44.22° and 55.10° match with FABr, and those at 18.4°, 23.58° and 39.65° match with $PbBr_2$. Although small amounts of precursors are present, the XRD patterns of $CsPbBr_3$ or $FAPbBr_3$ perovskites are not complicated by the precursor peaks. In other words, irrespective of the presence of small amounts of precursors, XRD data help us to characterize the perovskites. The morphologies of

the pellets and crystallites are examined by scanning electron microscopy (SEM) imaging. Representative SEM images of $FAPbBr_3$ samples are shown in the Supporting Information.

We characterized the optical properties of the pellets by estimating the bandgaps and PL spectra. Figure 2b and c shows the Tauc plots for $CsPbBr_3$ and $FAPbBr_3$ perovskites, respectively, which are obtained from the corresponding diffused reflectance spectra. The bandgaps are estimated at 2.30 eV for $CsPbBr_3$ and 2.21 eV for $FAPbBr_3$. These values are in good agreement with the solution processed nanocrystals[4c] or microcrystals[10] of $CsPbBr_3$ and $FAPbBr_3$. Furthermore, the PL maxima (ca 520 nm for $CsPbBr_3$ and ca 540 nm for $FAPbBr_3$, Figure 2d) of isolated crystallites in the samples are consistent with the estimated bandgap values (Figure 2b,c) and the literature reports.[4c,10] The red-shifted PL spectra of $FAPbBr_3$, when compared to that of $CsPbBr_3$ can be attributed to the difference in A-site cation and or difference in the degree of photon recycling. The A-site cation contributes indirectly to the bandgap, which is by the distortion of crystal lattice through the octahedral tilt leading to strong spinorbit coupling interactions.[11]

The PL behavior is visibly different for crystallites near the edge and center of the pellets (Figure 3a,b). At the edge, the reabsorption of emitted photons was low, and thus, the intensity of green emission was high. On the other hand, away from the edge, the sample showed yellow ($CsPbBr_3$) or orange ($FAPbBr_3$) emission, which suggests efficient photon recycling through closely-spaced energy states in these samples. To examine the existence of crystallites with

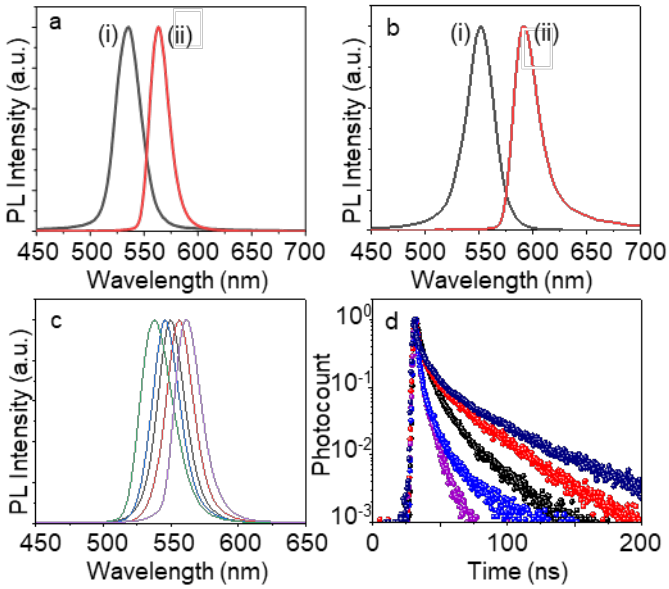

Figure 3. **The distribution of energy states and PL decays in perovskites.** (a,b) PL spectra of (a) $CsPbBr_3$ and (b) $FAPbBr_3$ perovskites recorded from (i) isolated crystallites and (ii) the core of the pellet. (c) PL spectra and (d) PL decay profiles (520 to 600 nm) of the randomly selected $FAPbBr_3$ crystallites. Here, the samples are minimally excited (0.05 mW) by a 400 nm fs laser.

distributed energy states in pure halide perovskites, we gently crushed a $FAPbBr_3$ pellet and collected the PL from different crystallites. As shown in Figure 3c, certain crystallites showed blue-shifted emission maxima (ca 530 nm), whereas certain other showed red-shifted maxima (ca 560nm). Further, crystallites with the red-shifted PL spectra showed longer PL lifetimes, while those with the blue-shifted PL spectra showed shorter PL lifetimes (Figure 3d). In other words, different PL maxima are accompanied with different PL lifetimes for crystallites collected from the pellet, and the long PL lifetime associated with the red-shifted emission helps us to consider nonradiative energy transfer in perovskite pellets. As with thick films and

single crystals of perovskites, photon recycling is often correlated with the reabsorption-emission processes,[3a-f] and the contribution of nonradiative energy transfer in this process is largely neglected. In addition to the above distribution of energy states, we find the PL lifetime values of the red-shifted and blue-shifted spectra are largely different. The red-shifted PL is delayed by 5.7 ns when compared to the blue-shifted one.

From the PL studies on different crystallites of a $CsPbBr_3$ or a $FAPbBr_3$ sample, which shows distribution of bandgaps with delayed emission, the contribution of nonradiative energy transfer in photon recycling is obvious. To clarify the roles of distinct energy states on energy transfer and photon recycling, we prepared mixed halide $FAPb(BrI)_3$ samples. We focused PL studies on the bromide-rich (500-575 nm) and iodide-rich (650-800 nm) regions and the bromide-iodide interface. Nonradiative energy transfer is substantiated from the PL intensity variation and the lifetime values in these regions (Figure 4a,b). Different regions of the mixed-halide pellet show different ratios of green and red emission intensities. This difference should be due to difference in the bromide-to-iodide ratios as well as difference in the efficiencies of nonradiative energy transfer. The overall effect of energy transfer should come from radiative and nonradiative processes, which are in addition to the migration of charge carriers. However, the contribution of energy transfer depends upon the degree of close-packing between the donor and acceptor. To clarify nonradiative energy transfer, we carried out the PL lifetime measurement in the 500 to 575 nm region for $FAPb(BrI)_3$ and compared it with a pure $FAPbBr_3$

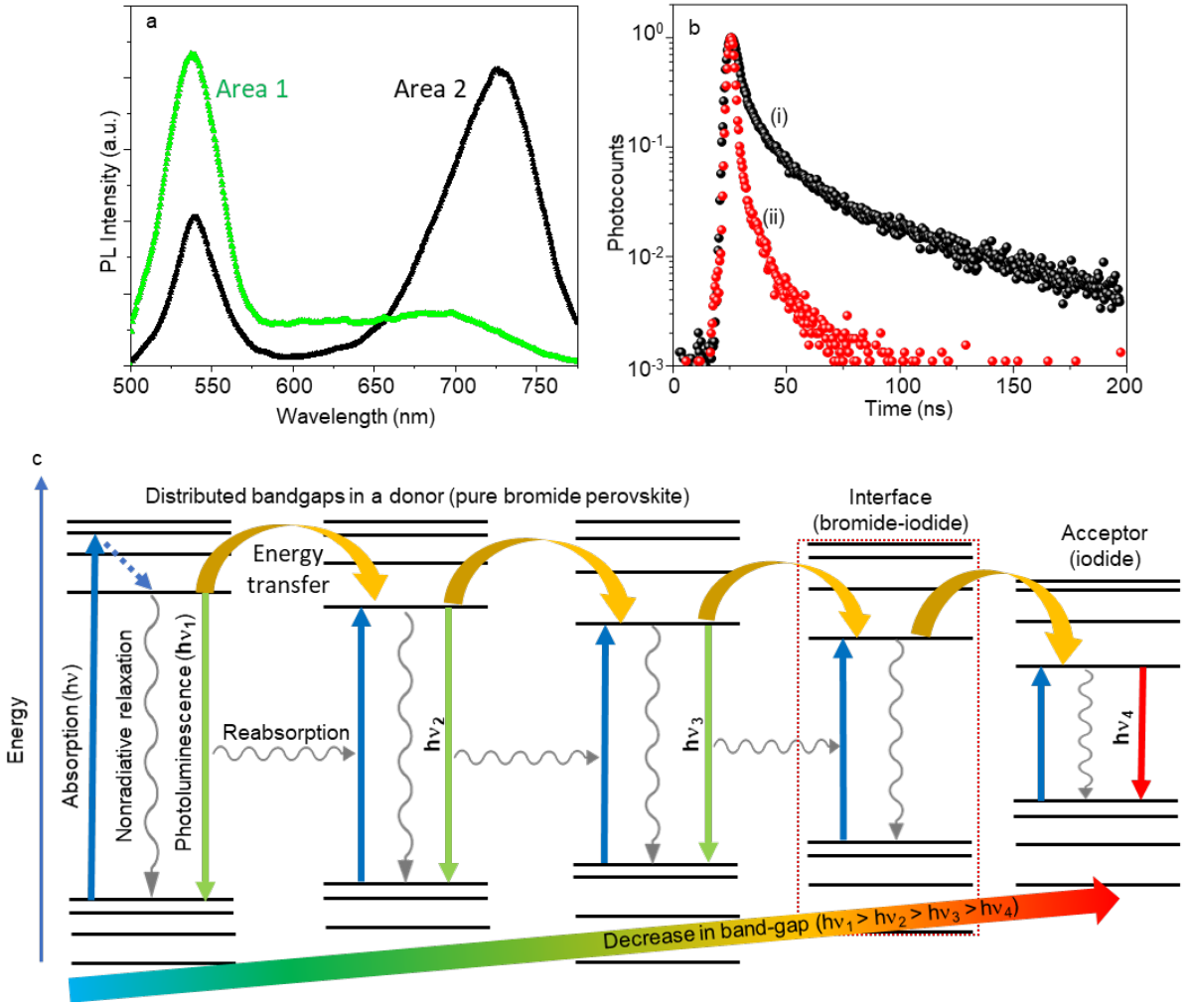

Figure 4. **Energy transfer in close-packed perovskite pellets.** (a) PL spectra of a $FAPb(BrI)_3$ perovskite sample collected from different areas. (b) PL decay profiles of (i) pure $FAPbBr_3$ perovskite and (ii) bromide (500-575 nm) region in a mixed halide $FAPb(BrI)_3$ pellet. (c) The mechanism of photon-recycling by the repeated radiative and nonradiative energy transfer processes in photoexcited perovskites.

sample (Figure 4b). Here, the bromide (500-575 nm) region in a mixed halide sample shows shorter lifetime (2.17 ns) when compared to the pure $FAPbBr_3$ sample (7.32 ns). This result helps us to confirm that the excited state of the bromide-rich part is deactivated by the iodide-rich parts. In other words, an efficient nonradiative energy transfer from the bromide to iodide regions is obvious.

We analyzed the extent of nonradiative energy transfer in mixed bromide-iodide perovskite sample by considering various radiative and nonradiative relaxation processes which follow their photoexcitation. Here, we compare the relaxation rate of the excited state of the bromide (500-575 nm) region in $FAPb(BrI)_3$ with the rate of pure $FAPbBr_3$ perovskite, which is by solving the equations (1) and (2).

$$\tau_0 = \frac{1}{k_\mathrm{r} + k_\mathrm{nr}} = \frac{1}{k_0} \tag{1}$$

$$\tau_1 = \frac{1}{k_\mathrm{r} + k_\mathrm{nr} + k_\mathrm{ET}} = \frac{1}{k_0 + k_\mathrm{ET}} \tag{2}$$

where, τ_0 and τ_1 are the average PL lifetimes of a pure $FAPbBr_3$ and the bromide (500-575 nm) region of the $FAPb(BrI)_3$ perovskite, respectively; k_r and k_nr are the rates of radiative and nonradiative relaxations, respectively; and k_ET is the rate of energy transfer. From the values of τ_0 and τ_1, we estimate k_ET at 3.24 x 10^8 s^{-1}, which is larger than the overall relaxation rate (k_0 = 1.36 x 10^8 s^{-1}) of pure $FAPbBr_3$. In other words, nonradiative energy transfer in the mixed halide sample is efficient.

The arrangement of energy states in close-packed perovskite crystallites is shown in Figure 4c, which illustrates various radiative and nonradiative relaxation processes including photon-recycling. Energy transfer from bromide to iodide regions is shown by placing the bandgaps of the donor and acceptor to the extreme left and right sides in Figure 4c, respectively, and the

closely-spaced states of the intermediate regions in the mixed halide compositions are shown in between. Radiative photon recycling follows the repeated absorption and emission of photons by the bromide, iodide and the intermediate regions. However, as discussed above, the radiative process alone cannot account for the increased rate of relaxation of the donor (bromide). In our study, the overall relaxation rate (k_r+k_{nr}+k_{ET}) of the bromide-rich part in $FAPb(BrI)_3$ is higher than pristine $FAPbBr_3$. Thus, in the mixed halide sample, the excited state of the donor is nonradiatively deactivated by the acceptor. The intermediate emission spectra in Figures 3 and energy bands in Figure 4 enable the efficient transfer of energy from the bromide to iodide regions.

In conclusion, we disclose photon-recycling in pure and mixed (bromide-iodide) halide perovskites pellets by the efficient nonradiative energy transfer process through the closely-spaced energy states. In pure and mixed halide perovskites, the closely-spaced bandgaps are validated based on distinct emission maxima and PL lifetime values. The close-packing of perovskite crystallites with the closely-spaced energy states in $CsPbBr_3$, $FAPbBr_3$ and $FAPb(BrI)_3$ helps us to clarify nonradiative energy transfer in perovskites.

EXPERIMENTAL SECTION

Synthesis of $CsPbBr_3$ and $FAPbBr_3$ perovskites

Required amounts of precursors (CsBr and $PbBr_2$ in 1:1.25 mol ratio, and FABr and $PbBr_2$ in

1.25:1.35 mol ratio) were powdered separately in a hand mortar and homogenously mixed by flipping up and down in a sample bottle. The precursor mixtures were loaded on a silicon rubber chamber with 20 mm diameter. Disc shaped pellets of perovskites were prepared in a hydraulic press by applying 2.4 GPa pressure vertically downward to the solid solutions of the precursors for 30 minutes. The pellets were stored in air-tight bottles for further studies.

Synthesis of $FAPb(BrI)_3$ perovskite pellet

Required amounts of precursors [FABr (0.75 mmol), $PbBr_2$ (0.75 mmol) and PbI_2 (0.25 mmol)] were weighed and powdered separately using a hand mortar. The powdered precursors were homogeneously mixed and loaded in a silicon rubber chamber. A pellet of $FAPb(BrI)_3$ perovskite was prepared by following the above method.

Methods

Kubelka- Munk diffused reflectance spectra were recorded in a UV-Vis spectrophotometer (Evolution 220, Thermo Fischer Scientific).

Time-resolved PL studies were carried out using a fluorescence microspectrometer. The excitation light source was femtosecond laser pulses (400 nm) from the second harmonic generator (SHG) crystal of an optical parametric amplifier (Coherent OPA) that was pumped with 800 nm pulses (150-fs, 200 kHz) from a regenerative amplifier (Coherent RegA). We used 76 MHz pulses from an oscillator (Coherent MIRA) for seeding RegA. The fluorescence

signals from the pellet and powder samples were collected through an objective lens (40x, Olympus UmPlan), filtered using a 460 nm long pass filter and directed to the entrance slit of an assembly of a polychromator (Chromex) and a streak-camera (Hamamatsu Photonics).

XRD measurements were carried out in a X-ray diffractometer (RINT 2200, Rigaku) using Cu Kα1 excitation (λ=1.5406 Å).

AUTHOR CONTRIBUTIONS

VB conceived the idea, BLSB prepared and characterized the perovskites. BLSB and SG conducted the optical studies, BLSB and SG prepared the manuscript draft, and BLSB SG and VB finalized the manuscript. All authors helped with data analysis and editing of the manuscript.

Notes

The authors declare no competing financial interest.

ACKNOWLEDGMENT

This work was carried out under the support of MEXT JSPS Grant-in-Aid for Scientific Research B (19H02550) and JSPS Grant-in-Aid for Specially Promoted Research (18H05205). It is also supported by the Dynamic Alliance for Open Innovation Bridging Human, Environment and Materials. BLSB and SG acknowledge MEXT scholarships for doctoral studies.

REFERENCES

1. a) W. Nie, H. Tsai, R. Asadpour, J.-C. Blancon, A. J. Neukirch, G. Gupta, J. J. Crochet, M. Chhowalla, S. Tretiak, M. A. Alam, H.-L. Wang, A. D. Mohite, *Science* **2015**, *347*, 522-525; b) N. K. Noel, B. Wenger, S. N. Habisreutinger, J. B. Patel, T. Crothers, Z. Wang, R. J. Nicholas; M. B. Johnston, L. M. Herz, H. J. Snaith, *ACS Energy Lett*. **2018**, *3*, 1233–1240; c) X. Zhang, W. Wang, B. Xu, S. Liu, H. Dai, D. Bian, S. Chen, K. Wang, X.W. Sun, *Nano Energy* **2017**, *37*, 40–45; d) S. T. Ochsenbein, F. Krieg, Y. Shynkarenko, G. Rainò, M. V. Kovalenko, *ACS Appl. Mater. Interfaces* **2019**, *11*, 21655–21660; e) S. Yakunin, Protesescu, L. Yakunin, F. Krieg, M. I. Bodnarchuk, G. Nedelcu, M. Humer, G. De Luca, M. Fiebig, W. Heiss, M. V. Kovalenko, *Nat. Commun.* **2015**, *6*, 8056; f) A. Zhizhchenko, S. Syubaev, A. Berestennikov, A. V. Yulin, A. Porfirev, A. Pushkarev, I. Shishkin, K. Golokhvast, A. A Bogdanov, A. A. Zakhidov, et al., *ACS Nano* **2019**, *13*, 4140–4147; g) J.-H. Cha, J. H. Han, W. Yin, C. Park, Y. Park, T. K. Ahn, J. H. Cho, D.-Y. Jung, *J. Phys. Chem. Lett.* **2017**, *8*, 565–570; h) F. Zhang, B. Yang, K. Zheng, S. Yang, Y. Li, W. Deng, R. He, *Nano-Micro Lett.* **2018**, *10*, 43.
2. a) Q. Dong, Y. Fang, Y. Shao, P. Mulligan, J. Qiu, L. Cao, J. Huang, *Science* **2015**, *347*, 967–970; b) Y. Bi, E. M. Hutter, Y. Fang, Q. Dong, J. Huang, T. J. Savenije, *J. Phys. Chem. Lett.* **2016**, *7*, 923–928.

3. a) T. Kirchartz, F. Staub, U. Rau, *ACS Energy Lett.* **2016**, *1*, 731–739; b) L. M. Pazos-Outón, M. Szumilo, R. Lamboll, J. M. Richter, M. Crespo-Quesada, M. Abdi-Jalebi; H. J. Beeson, M. Vrućinić, M. Alsari, H. J. Snaith, B. Ehrler, R. H. Friend, F. Deschler, *Science* **2016**, *351*, 1430–1433; c) T. W. Crothers, R. L. Milot, J. B. Patel, E. S. Parrott, J. Schlipf, P. Müller-Buschbaum; M. B. Johnston, L. M. Herz, *Nano Lett.* **2017**, *17*, 5782–5789; d) I. Dursun, Y. Zheng, T. Guo, M. De Bastiani, B. Turedi, L. Sinatra, M. A. Haque, B. Sun, A. A. Zhumekenov, M. I. Saidaminov, F. P. G. de Arquer, E. H. Sargent, T. Wu, Y. N. Gartstein, O. M. Bakr, O. F. Mohammed, A. V. Malko, *ACS Energy Lett.* **2018**, *3*, 1492–1498; e) H. Diab, C. Arnold, F. Ledée, G. Trippe-Allard, G. Delport, C. Vilar, F. Bretenaker, J. Barjon, J.-S. Lauret, E. Deleporte, D. Garrot, *J. Phys. Chem. Lett.* **2017**, *8*, 2977−2983; f) S. G. Motti, T. Crothers, R. Yang, Y. Cao, R. Li, M. B. Johnston, J. Wang, L. M. Herz, *Nano Lett.* **2019**, *19*, 3953–3960.

4. a) N. Wang, L. Cheng, R. Ge, S. Zhang, Y. Miao, W. Zou, C. Yi, Y. Sun, Y. Cao, R. Yang, et al., *Nat. Photonics* **2016**, *10*, 699–705; b) A. M. E. Bouduban, A. Burgos-Caminal, R. Ossola, J. Teuscher, J.-E. Moser, *Chem. Sci.* **2017,** *8*, 4371–4380; c) S. Ghimire, L. Chouhan, Y. Takano, K. Takahashi, T. Nakamura, K. Yuyama, V. Biju, *ACS Energy Lett.* **2019**, *4*, 133–141; d) S. Ghimire, V. C. Nair, C. Muthu, K. Yuyama, M. Vacha, V. Biju, *Nanoscale* **2019**, *11*, 9335–9340.

5. a) M. Braun, W. Tuffentsammer, H. Wachtel, H. C. Wolf, *Chem. Phys. Lett.* **1999**, *303*,

157–164; b) N. J. L. K. Davis, F. J. de la Peña, M. Tabachnyk, J. M. Richter, R. D. Lamboll, E. P. Booker, F. W. R. Rivarola, J. T. Griffiths, C. Ducati, S. M. Menke, *J. Phys. Chem. C* **2017**, *121*, 3790–3796.

6. S. Ghimire, K. Takahashi, Y. Takano, T. Nakamura, V. Biju, *J. Phys. Chem. C* **2019**, *123*, doi.org/10.1021/acs.jpcc.9b07003.
7. a) C. C. Stoumpos, C. D. Malliakas, M. G. Kanatzidis, *Inorg. Chem.* **2013**, *52*, 9019–9038. b) D. Prochowicz, M. Franckevičius, A. M. Cieślak, S. M. Zakeeruddin, M. Grätzel, J. Lewiński, *J. Mater. Chem. A* **2015**, *3*, 20772–20777 c) L. Protesescu, S. Yakunin, O. Nazarenko, D. N. Dirin, M. V. Kovalenko, *ACS Appl. Nano Mater.* **2018**, *1*, 1300–1308.
8. G. Serghiou, A. Zerr, R. Boehler, *Science* **1998**, *280*, 2093–2095.
9. Y.-L. Tong, Y.-W. Zhang, K. Ma, R. Cheng, F. Wang, S. Chen, *ACS Appl. Mater. Interfaces* **2018**, *10*, 31603–31609.
10. a) M. I. Saidaminov, A. L. Abdelhady, G. Maculan, O. M. Bakr, *Chem. Comm.* **2015**, *51*,17658–17661; b) S. Kondo, H. Nakagawa, T. Saito, H. Asada, *Current Applied Physics* **2004,** *4*, 439–444.
11. a) C. C. Stoumpos, M. G. Kanatzidis, *Acc. Chem. Res.* **2015**, *48*, 2791–2802; b) A. Amat, E. Mosconi, E. Ronca, C. Quarti, P. Umari, M. K. Nazeeruddin, M. Grätzel, F. D. Angelis, *Nano Lett.* **2014**, *14*, 3608–3616.

TOC Graphic

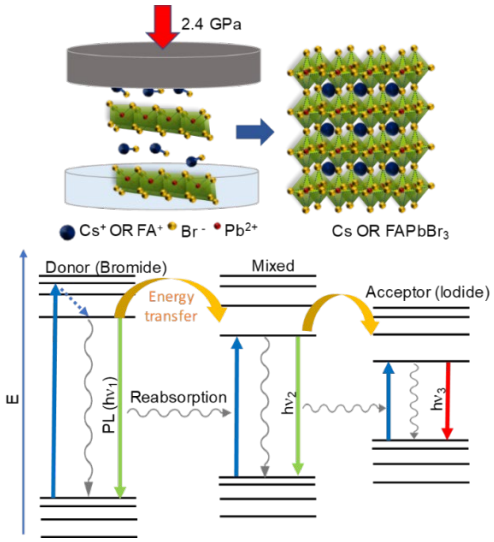
2.4 GPa
Cs⁺ OR FA⁺
Br⁻
Pb²⁺
Cs OR FAPbBr3
Donor (Bromide)
Energy transfer
Mixed
Acceptor (Iodide)
E
PL (hν1)
Reabsorption
hν2
hν3